

Unravelling biotoxicity of graphdiyne: Molecular dynamics simulation of the interaction between villin headpiece protein and graphdiyne

Bei-Wei Zhang(张贝薇), Bing-Quan Zhang(张兵权), Zhi-Gang Shao(邵志刚), and Xianqiu Wu(吴先球)

Citation: Chin. Phys. B, 2024, 33 (**11**): 118102. DOI: 10.1088/1674-1056/ad7af5
Journal homepage: http://cpb.iphy.ac.cn; http://iopscience.iop.org/cpb

What follows is a list of articles you may be interested in

Molecular dynamics study of thermal conductivities of cubic diamond, lonsdaleite, and nanotwinned diamond via machine-learned potential

Jia-Hao Xiong(熊佳豪), Zi-Jun Qi(戚梓俊), Kang Liang(梁康), Xiang Sun(孙祥), Zhan-Peng Sun(孙展鹏), Qi-Jun Wang(汪启军), Li-Wei Chen(陈黎玮), Gai Wu(吴改), and Wei Shen(沈威)
Chin. Phys. B, 2023, 32 (**12**): 128101. DOI: 10.1088/1674-1056/ace4b4

Thermal and mechanical properties and micro-mechanism of SiO_2/epoxy nanodielectrics

Tian-Yu Wang(王天宇), Gui-Xin Zhang(张贵新), and Da-Yu Li(李大雨)
Chin. Phys. B, 2021, 30 (**12**): 128101. DOI: 10.1088/1674-1056/abff2c

Prediction of structured void-containing 1T-$PtTe_2$ monolayer with potential catalytic activity for hydrogen evolution reaction

Bao Lei(雷宝), Yu-Yang Zhang(张余洋), Shi-Xuan Du(杜世萱)
Chin. Phys. B, 2020, 29 (**5**): 058104. DOI: 10.1088/1674-1056/ab8203

Density functional calculations of efficient H_2 separation from impurity gases (H_2, N_2, H_2O, CO, Cl_2, and CH_4) via bilayer g-C_3N_4 membrane

Yuan Guo(郭源), Chunmei Tang(唐春梅), Xinbo Wang(王鑫波), Cheng Wang(王成), Ling Fu(付玲)
Chin. Phys. B, 2019, 28 (**4**): 048102. DOI: 10.1088/1674-1056/28/4/048102

A simulation study of water property changes using geometrical alteration in SPC/E

Ming-Ru Li(李明儒), Nan Zhang(张楠), Feng-Shou Zhang(张丰收)
Chin. Phys. B, 2018, 27 (**8**): 083103. DOI: 10.1088/1674-1056/27/8/083103

Unravelling biotoxicity of graphdiyne: Molecular dynamics simulation of the interaction between villin headpiece protein and graphdiyne

Bei-Wei Zhang(张贝薇)[1], Bing-Quan Zhang(张兵权)[2], Zhi-Gang Shao(邵志刚)[1,2,†], and Xianqiu Wu(吴先球)[1,2]

[1] *Guangdong Basic Research Center of Excellence for Structure and Fundamental Interactions of Matter, Guangdong Provincial Key Laboratory of Quantum Engineering and Quantum Materials, School of Physics, South China Normal University, Guangzhou* 510006, *China*

[2] *Guangdong–Hong Kong Joint Laboratory of Quantum Matter, Frontier Research Institute for Physics, South China Normal University, Guangzhou* 510006, *China*

(Received 21 May 2024; revised manuscript received 16 July 2024; accepted manuscript online 14 September 2024)

Recently, there has been a growing prevalence in the utilization of graphdiyne (GDY) in the field of biomedicine, attributed to its distinctive physical structure and chemical properties. Additionally, its biocompatibility has garnered increasing attention. However, there is a lack of research on the biological effects and physical mechanisms of GDY-protein interactions at the molecular scale. In this study, the villin headpiece subdomain (HP35) served as a representative protein model. Molecular dynamics simulations were employed to investigate the interaction process between the HP35 protein and GDY, as well as the structural evolution of the protein. The data presented in our study demonstrate that GDY can rapidly adsorb HP35 protein and induce denaturation to one of the α-helix structures of HP35 protein. This implies a potential cytotoxicity concern of GDY for biological systems. Compared to graphene, GDY induced less disruption to HP35 protein. This can be attributed to the presence of natural triangular vacancies in GDY, which prevents π–π stacking action and the limited interaction of GDY with HP35 protein is not conducive to the expansion of protein structures. These findings unveil the biological effects of GDY at the molecular level and provide valuable insights for the application of GDY in biomedicine.

Keywords: graphdiyne, villin headpiece, molecular dynamics simulation, biotoxicity

PACS: 81.05.U–, 87.10.Tf, 87.14.E–, 87.15.bd **DOI:** 10.1088/1674-1056/ad7af5

1. Introduction

With the rapid development of nanotechnology and nanoscience, nanomaterials are widely used in various industries due to their unique physicochemical properties, especially the quantum and surface effects exhibited at the nanoscale. Particularly in the realm of nano-biomedicine, such as gene delivery, cellular imaging, oncology treatment, and bio-experimental techniques.[1–3] Inevitably, in these applications, nanomaterials are able to interact directly with biological cells, resulting in a range of biological effects. The cell membrane represents the initial barrier of protection for cells within an organism. Xu *et al*. conducted research into the interaction mechanism of single-stranded DNA (ssDNA) and single-stranded RNA (ssRNA) in lipid nanoparticles (LNPs) with a phospholipid bilayer and found that Ca^{2+} and Mg^{2+} could facilitate the interaction.[4] Luo *et al*. identified two patterns of binding between C_3N and small intestinal epithelial cell membrane: insertion or coverage.[5] Furthermore, they demonstrated that glycosphingolipids prevented C_3N from inserting into the membrane. In addition, Wu *et al*. investigated the adsorption of double-stranded DNA (dsDNA) molecules of different lengths on the graphene oxide (GO) surface.[6] Ma *et al*. demonstrated that the adsorption of ssDNA with GO was most stable when the degree of oxidation of GO was approximately 15%, as this resulted in the highest number of π–π stacking interactions between the two components.[7] Zhang *et al*. investigated the adsorption of DNA by a novel two-dimensional (2D) carbon nanomaterial, biphenylene network, and found that the biphenylene network can denature the structure of ssDNA, whereas it displays good biocompatibility with dsDNA.[8] Nanomaterials also have the potential to alter the secondary, tertiary, or quaternary structure of proteins.[9] For instance, Zhang *et al*. observed that both phosphene and graphene could disrupt the secondary structure of the villin headpiece protein, with graphene causing more severe disruption to the protein's structure.[10] Gu *et al*. discovered that the surface of graphene materials have the capability to trap biomolecules, potentially leading to alterations in the tertiary structure of proteins.[11] Babadaei *et al*. discovered that graphene oxide nanosheets affected the Tyr residues near human haemoglobin, leading to changes in the quaternary structure.[12] Prior investigations have indicated that, contingent on the proteins involved, these carbon nanomaterials may serve as drug carriers or exhibit potential toxic effects.[13–17] Hence, conducting a comprehensive and in-depth study on the biocompatibility of carbon nanomaterials is of paramount im-

†Corresponding author. E-mail: zgshao@scnu.edu.cn

© 2024 Chinese Physical Society and IOP Publishing Ltd

portance. Due to the severe challenges associated with conducting detailed experiments to explore the molecular-scale interaction mechanisms between carbon nanomaterials and biomolecules, employing numerical simulations becomes imperative. These simulations can be effectively combined with experimental data to guide practical applications. Related literatures indicate that computational simulations can be advantageous in certain contexts.[18,19]

In recent years, there has been a rapid development in carbon nanostructured materials. Owing to their abundant carbon chemical bonds, large conjugated systems, wide facet spacing, and excellent chemical stability, these materials have garnered increasing attention in various fields, including electronics, optics, energy, catalysis, biomedicine, etc.[20–27] Graphdiyne (GDY) is a novel 2D carbon-based nanomaterial that is an allotrope of carbon similar to graphene. It comprises planar structures of benzene and alkyne units with two types of carbon atoms: sp- and sp^2-hybrid carbon atoms, featuring abundant chemical bonding, large π–π conjugated systems, a naturally porous structure, an intrinsic bandgap, high carrier mobility, surface inhomogeneous charge distribution, excellent mechanical properties, and high surface activity.[28–30] Since their initial experimental synthesis in 2010, GDY and its derivatives have found successful applications in energy, catalysis, environmental, and biomedical domains owing to their exceptional properties.[31–37] The wide range of applications also substantially elevates the risk of human exposure, potentially leading to adverse effects on human health. Hence, there is a growing urgency and necessity to investigate the interaction mechanism of GDY with biomolecules and to further explore the potential toxicity of GDY.

Relevant studies have indicated that the hydrophobicity of graphyne nanosheets could directly interfere with the normal function of proteins. For example, Feng *et al*. explored the binding of graphyne nanosheets and graphyne quantum dots to calmodulin, revealing a potential molecular mechanism underlying graphyne cytotoxicity.[38] Gu *et al*. demonstrated that graphyne was able to insert itself into cellular membranes and extract phospholipids due to its hydrophobicity.[39] This suggests that graphyne could be used as a potential antimicrobial agent. Luan *et al*. employed molecular dynamics simulations to explore the potential toxicity of graphyne by interfering with protein–protein interactions (PPI). Their findings indicated that, owing to dispersive and hydrophobic interactions of graphyne with hydrophobic residues at the dimer interface, graphyne can disrupt PPI by cleaving the protein–protein interface and separating the protein complex into non-contacting materials.[40] Zhu *et al*. experimentally confirmed that GDY exhibited higher antibacterial activity than GDY oxide.[41]

Despite these efforts, the detailed molecular interactions between GDY and proteins continue to elude comprehensive understanding. In this study, we employed all-atom molecular dynamics (MD) simulations to scrutinize the adsorption process and structural evolution of the helix-rich villin headpiece subdomain protein (HP35) with GDY. Our results show that HP35 protein adsorbed on GDY rapidly and the binding site was relatively stable. The interaction between HP35 protein and GDY predominantly relied on van der Waals (vdW) interactions. Upon binding to GDY, the α-helix 1 fragment of the HP35 protein underwent denaturation, resulting in the loss of part of the secondary structure. This implies the potential biotoxicity of GDY at the molecular level. However, GDY exhibits lower biotoxicity than graphene, attributable to its natural triangular vacancy structure.[42] The presence of extensive vacancies hampers the ability of aromatic residues in HP35 to form π–π stacking structures with the six-membered ring in GDY. Additionally, the limited interaction of GDY with HP35 protein is not conducive to the expansion of protein structures. Our findings contribute to a deeper understanding of the interaction mechanism between GDY and proteins, providing insights that can guide the application of GDY in biomedical fields.

2. Model and method

The GDY nanosheet monolayer is an all-carbon structure with a 2D planar network formed by the conjugated linking of benzene rings through 1,3-diyne bonds, as shown in Fig. 1(a). The GDY model employed in our simulations is a nanosheet with dimensions of 6.0 nm×5.5 nm and comprises 756 carbon atoms. In GDY, the carbon atoms are modeled as uncharged Lennard–Jones (LJ) particles.[39] The vdW parameters for the sp carbon atoms are $\sigma_{cc} = 3.4$ Å and $\varepsilon_{cc} = 0.210$ kcal/mol, while for the sp^2 carbon atoms are $\sigma_{cc} = 3.4$ Å and $\varepsilon_{cc} = 0.086$ kcal/mol. The HP35 protein structure was obtained from the Protein Data Bank (PDB code: 1YRF). Its widespread use in modeling nanomaterials and proteins is attributed to its small size and properties commonly found in globular proteins, and thus there is a diverse array of findings for comparative analysis.[10,11,42–50] The native structure of the HP35 protein consists of 35 residues, with residues 4–10 constituting the helical fragment α1, residues 15–19 constitute helical fragment α2, and residues 23–32 helical fragment α3, as shown in Fig. 1(b). Initially, we positioned the protein above the GDY at a distance of 2 nm, as illustrated in Fig. 1(c). Water was modelled using tip3p water.[51] Cl^- ions are essential electrolytes in living organisms, and we added Cl^- ions to balance the excess positive charge in the simulated system in line with the physiological environment. Therefore, 2 Cl^- ions were added to undergo electrostatic interactions with the HP35 protein, which served to neutralize the charge of the HP35 protein. (Cl^- ions may also be adsorbed on the surface of GDY due to vdW interaction. Figure S1 illustrates that the distance

between the Cl^- ions and GDY is variable, indicating that the Cl^- ions are in a free state in an aqueous solvent and does not bind to GDY, nor affect the surface properties of GDY). The complexes were situated in a 7.0 nm×6.5 nm×6.5 nm box, with water serving as the solvent, and periodic boundary conditions were applied in all three directions.

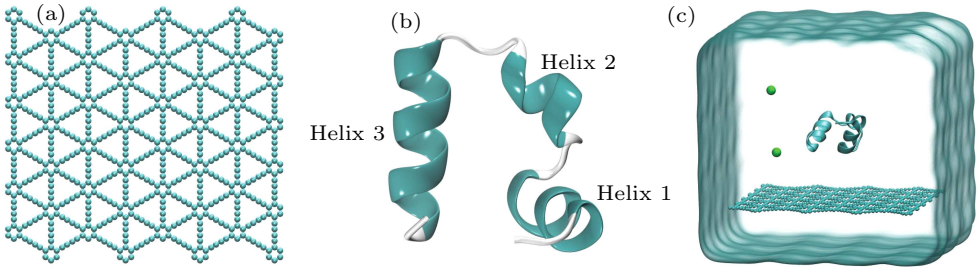


Fig. 1. Conformation diagram of (a) GDY and (b) HP35 protein. (c) The initial structure diagram of HP35 protein and graphdiyne in a water box. Here, the green balls are Cl^- ions.

All MD simulations were performed using the GROMACS software package, and the force field was described using AMBER99SB.[52,53] The VMD software was utilized for visualizing the molecular structure.[54] Remote electrostatic interactions were calculated using the particle lattice Ewald method.[55,56] The cut-off distance for vdW interactions was 1.2 nm. All solute bonds involving hydrogen atoms were constrained by the LINCS algorithm.[57] During the run, the energies of systems were minimised and subsequent equilibration for 1 ns, employing the NVT and NPT ensembles, respectively. Throughout the equilibration process, the heavy atoms of the proteins were restrained. The temperature was kept at 300 K using the v-rescale method, while the pressure of the system was controlled to one atmosphere through the Parrinello–Rahman algorithm.[58,59] Subsequently, simulations lasting 600 ns were conducted for the system in the NVT ensemble, with a time step of 2.0 fs, and data were collected every 10 ps.

3. Results and discussion

First, we explored the dynamic adsorption process of HP35 protein on the GDY surface. Conformation diagrams at crucial moments during the simulation are depicted in Figs. 2(a)–2(f). At 0 ns, the centre-of-mass distance between the HP35 protein and GDY was 2 nm, and the protein was parallel to the GDY surface. Notably, the contact area at this time was 0 nm^2, signifying adequate separation between the protein and GDY. From the distance between the protein and GDY in Fig. 3(a) and the contact area in Fig. 3(b), it can be seen that the distance between the protein and GDY in the z direction firstly increased transiently and then rapidly decreased to 0.9 nm, and the area increased from 0 to about 6 nm^2 within the 0–9 ns timeframe. From the conformation diagram at 10 ns, it is evident that the α-helix 1 structure of the protein was turned, but the secondary structure was not mutated. At about 230 ns, the distance between the protein and GDY in the z direction changed little, but the contact area increased further. Additionally, in the conformational diagram at 300 ns, it is evident that the α-helix 1 of the protein underwent mutation. This implies that GDY has the potential to disturb the protein structure, resulting in nanotoxicity. Notably, around 335 ns, there was only a slight rebound in the contact area, signifying the relatively stable adsorption of GDY on the HP35 protein. Correspondingly, in the conformational diagram at 400 ns, there was no discernible alteration in the protein conformation compared to the state at 300 ns. Subsequently, the contact area and distance exhibited minimal oscillation throughout the simulation, and the alterations in the relative distances between the protein and GDY in all three directions (xyz) fluctuated within the range of 0.5 nm. The conformation of the HP35 protein had essentially ceased to evolve, as depicted in Figs. 2(d) and 2(e), implying that a simulation duration of 600 ns adequately represents the kinetic characteristics of protein adsorption on GDY.

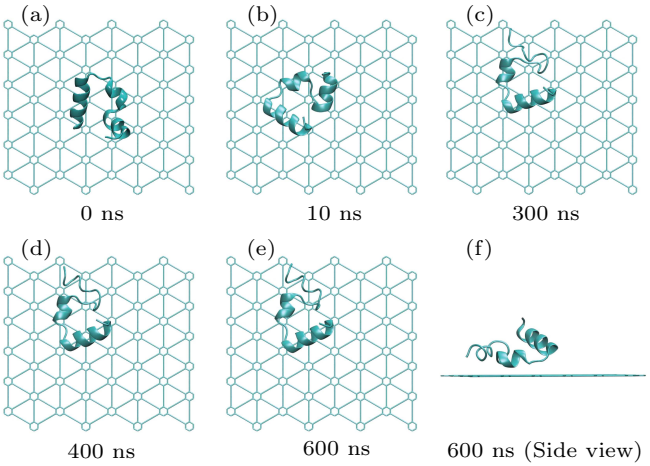


Fig. 2. Conformation diagram of HP35 protein and GDY at different critical time scales during the simulation.

Second, we discussed the overall conformational changes of the protein during the adsorption process. The root-mean-square deviation (RMSD) depicted in Fig. 4(a) reflects the degree of change in protein structure. The radius of gyration (R_g) of the protein, as depicted in Fig. 4(b), characterizes the volume and shape of the protein molecule. The larger the radius

of gyration of the same system, the more swollen the protein is. Figure 4 shows an evident abrupt change in the RMSD of the protein near 230 ns. However, the magnitude of this change fluctuated only in the range of 0.17 to 0.44. In order to provide a more accurate description of the variation of R_g, we have synthesized the curve of R_g into a linear function. The function and the fitted plot line are shown in Fig. S2 in the supporting information. The results of the function indicate that R_g has a tendency to increase, which suggests that the overall structure of the protein is undergoing a slight expansion. The shape of the HP35 protein is asymmetric, and the distribution of its mass is not uniform in three directions. Consequently, when the protein is rotated in the x–y plane at about 20 ns, 130 ns, 210 ns, and 330 ns, R_{g_x} and R_{g_y} exhibit considerable fluctuations with opposing values. The protein hardly rotates in the x–z and y–z planes, but there is a slight expansion over time along the z direction, resulting in insignificant fluctuations in R_{g_z}. These findings suggest that the adsorption of proteins on the GDY surface results in the disruption of the protein structure, with a relatively low intensity of destruction. Additionally, both the RMSD and R_g values exhibited stability at the conclusion of the simulation, indicating that 600 ns is sufficient to reflect the effects caused by GDY on the protein structure.

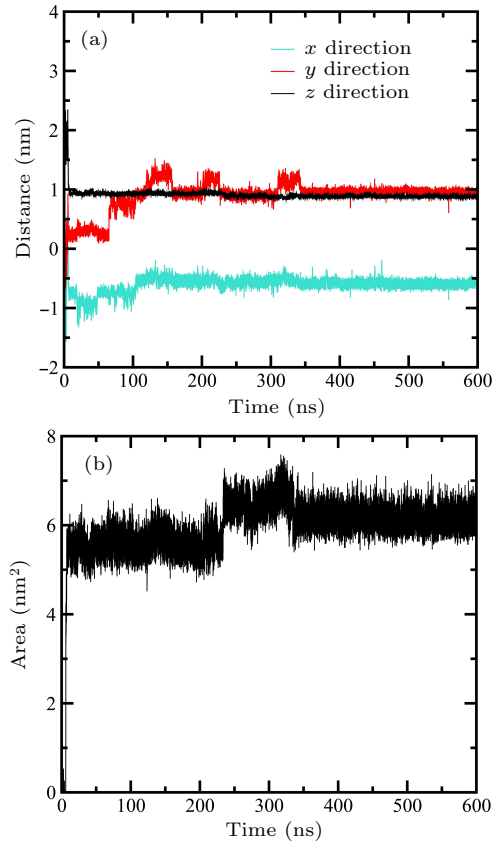


Fig. 3. (a) Diagram of the distance between the protein and GDY over time. (b) Diagram of the contact area between the protein and GDY over time.

Next, we analyzed the alterations in the internal secondary structure of the protein throughout the simulation. From Fig. 5, we can see that α-helix 2 and α-helix 3 remained structurally stable during the simulation. Nevertheless, α-helix 1 had been unfolded around 230 ns. Most α-helix 1 had been changed to 3_{10}-helix and turns. In conjunction with the abrupt change in the RMSD value at the same time point, it suggests that the structural changes in the protein during this period originated from the denaturation of the secondary structure of α-helix 1.

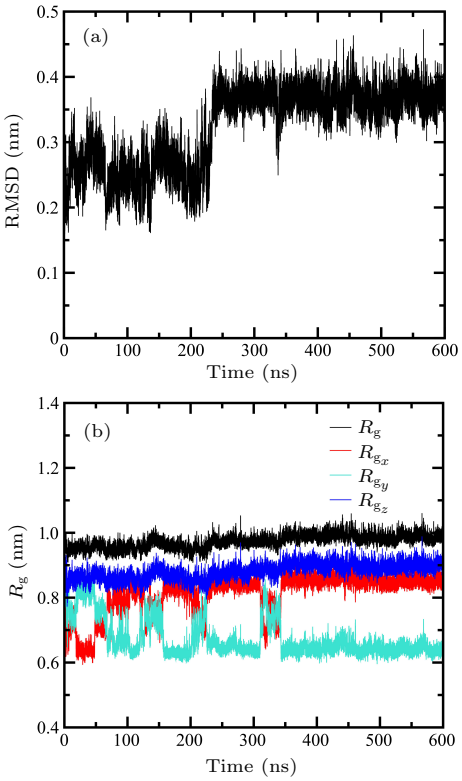


Fig. 4. (a) Diagram of the root-mean-square deviation of the protein over time. (b) Diagram of the radius of gyration of the protein over time.

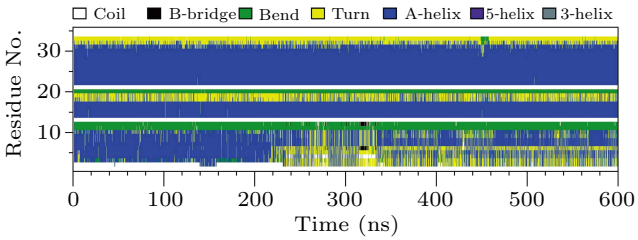


Fig. 5. Diagram of the secondary structure of HP35 protein during the simulation, obtained by the DSSP program.[60]

The Ramachandran plot is a method used to visualize the extent of protein structure disruption.[61] The extent of conformational changes in protein residues upon adsorption of the HP35 protein on the GDY surface is assessed by plotting the reasonability of dihedral angles ψ and ϕ for individual residues in the protein backbone. We sampled the protein conformation after the equilibrium of the simulation process, but essentially obtained the same result, so we plotted the Ramachandran plot of the protein with 600 ns as an example. Figure 6 reveals the presence of 30 non-glycine and non-proline residues in the main chain of the HP35 protein. In the initial state, all residues were positioned in the "most favoured

regions" (A, B, L), as shown in Fig. 6(a). Upon reaching system stability, 86.7% of residues were situated in the "most favoured regions", 13.3% were in the "additional allowed regions" (a, b, l, p), and none of them were in the "generously allowed regions" (~a, ~b, ~l, ~p) or "disallowed regions", as shown in Fig. 6(b). In comparison to the initial state, the dihedral angle distribution of the HP35 protein at 600 ns exhibited significant changes, suggesting that the adsorption of GDY induces alterations in the conformation of the HP35 protein. The dihedral angle distribution of four residues, namely Leu1, Lys7, Ala8, and Thr13, fell within the "additional allowed regions". Notably, residues Lys7 and Ala8 belong to the α-helix 1, indicating that the denaturation of the α-helix 1 structure may be attributed to alterations in the dihedral angle of the pertinent residues. Nevertheless, only four out of the thirty main chain residues were outside the "most favoured regions", suggesting that the damage inflicted by GDY on the HP35 protein was not severe.

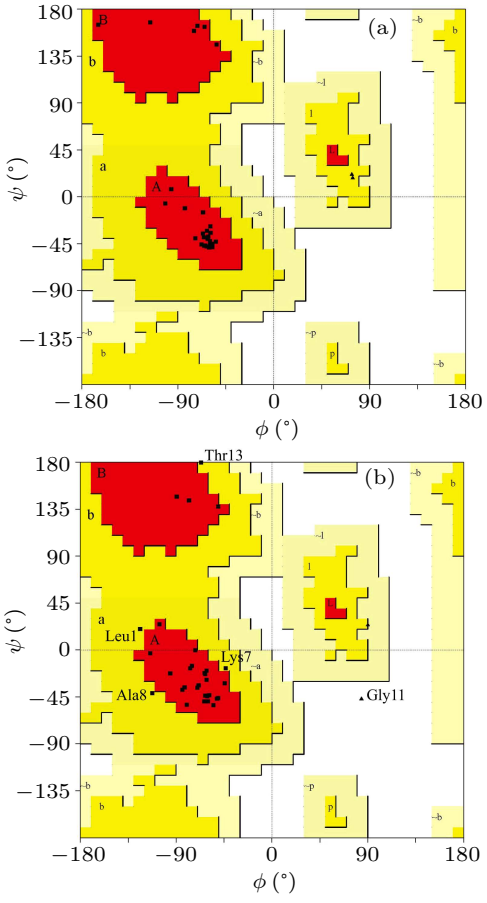


Fig. 6. The Ramachandran plot of HP35 protein in (a) 0 ns and (b) 600 ns. The images were created with the Procheck program.[62]

Finally, we explored the primary interaction forces between GDY and HP35 protein. Since the C atoms in GDY are uncharged, electrostatic interactions are not taken into consideration. The variation of vdW interaction energy between GDY and the protein with time is shown in Fig. 7. The figure illustrates that the trend of vdW interaction energy closely mirrors that of the contact area, suggesting that vdW interaction energy constitutes the primary force driving the adsorption of HP35 protein on GDY.

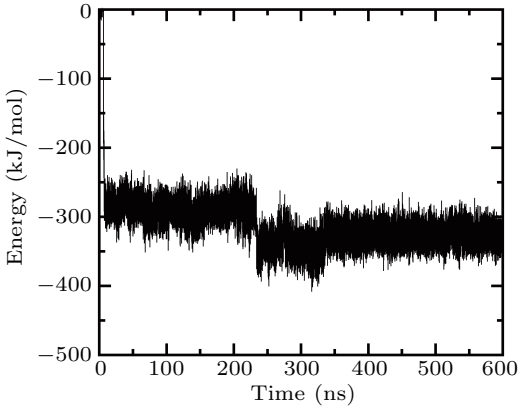
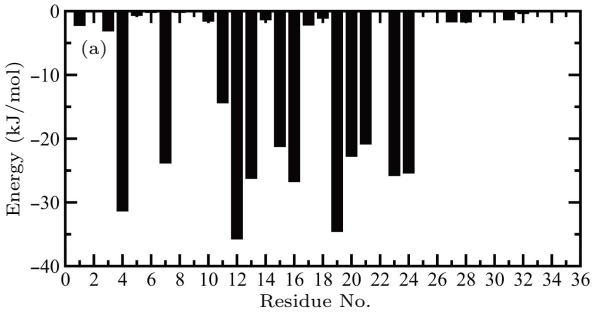


Fig. 7. Diagram of the van der Waals interaction energy between the protein and GDY over time.

We further calculated the average vdW interaction energy between each residue and GDY and analyzed the binding characteristics of aromatic residues with GDY, as shown in Fig. 8. For the HP35 protein, as shown in Fig. 8(a), the average vdW energy of α-helix 3 residues was close to zero, indicating that these residues did not bind to GDY. Correspondingly, figure 2(f) also indicates that α-helix 3 remains relatively distant from GDY after the system reaches stability. The average vdW energies between residues Glu4, Lys7, Met12, Thr13, Ser15, Ala16, Asn19, Leu20, Pro21, Trp23, and Lys24 and GDY were relatively large (> 20 kJ/mol), suggesting that these residues are adsorbed to GDY. Zuo *et al*. discovered that aromatic residues Phe10, Trp23, and Phe35 engage in π–π stacking interactions with graphene, which plays a key role in the adsorption of HP35 protein with graphene. The addition of graphene resulted in the loss of the majority of the secondary structure of the HP35 protein, specifically in α-helix 1 and α-helix 3.[42] This finding aligns with the results observed by Zhou *et al*. when the graphene size was sufficiently large.[50] In our study, only α-helix 1 structure was denatured. In contrast, the impact of GDY on the secondary structure of HP35 protein was considerably less pronounced. In the graphene-HP35 system, the RMSD of the HP35 protein finally converged at approximately 0.75 nm, while in the GDY-HP35 system, the RMSD of the HP35 protein finally converged at approximately 0.4 nm. It is evident that the denaturation of the overall structure of the HP35 protein by GDY is not as pronounced as that observed with graphene. Unlike graphene, GDY comprises not only hexagonal rings but also large triangular rings. This structural feature prevented the five aromatic residues Phe6, Phe10, Phe17, Trp23, and Phe35 in the

HP35 protein from engaging in π–π stacking interactions with the hexagonal rings of GDY. Despite the residue Trp23 had a large vdW energy with GDY, the residue was adsorbed to the triangular vacancies on the surface of GDY and failed to form a π–π stacking structure with the hexagonal ring of GDY, as depicted in Fig. 8(b). The vdW interaction energy between graphene and HP35 proteins was demonstrated by Zhang *et al*. to be stabilized at approximately −672 kJ/mol following simulated convergence.[10] In contrast, our experimental results indicate a stabilization of approximately −325 kJ/mol. The restricted π–π stacking and vdW interactions between the HP35 protein and GDY may have constrained the expansion of the protein structure, resulting in the denaturation of HP35 protein by GDY being less intense than that of graphene.



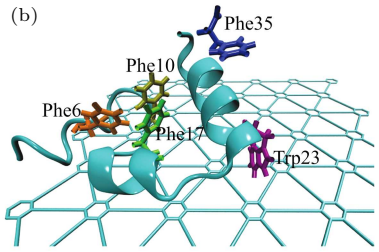


Fig. 8. (a) Diagram of the van der Waals interaction energy between each residue of HP35 and GDY was averaged from 500 ns to 600 ns. (b) Conformation diagram of HP35 protein and GDY at 600 ns, where coloured loops indicate aromatic residues.

4. Conclusions

This work investigates the interaction between planar GDY nanomaterials and the HP35 protein through molecular dynamics simulations. The adsorption characteristics of HP35 protein on GDY were revealed by analyzing the conformational diagrams, adsorption distance, contact area and interaction energies, as well as the root mean square deviation, radius of gyration, secondary structure and Ramachandran plot of the protein. It was found that HP35 protein could be adsorbed on the surface of GDY rapidly due to vdW interactions. HP35 protein exhibited slight vibration when adsorbed on the surface of GDY. After binding to GDY, α-helix 1 in HP35 protein underwent denaturation, while the structures of the other two α-helices remained intact. Our results suggest that GDY may pose potential molecular-level toxicity to biological tissues. Comparing our results with the interaction between HP35 protein and graphene, we observed that the extent of HP35 protein disruption by GDY was relatively low. This can be attributed to the fact that the inherent triangular vacancies in GDY impede π–π stacking interactions, and that the limited interactions are not favourable to the expansion of the protein structure. Our study elucidates the mechanism of GDY-protein interactions at the molecular level, advances the exploration of biotoxicity in other related nanomaterials within the field of nanotoxicology, and provides theoretical support for better application of GDY in biomedical fields.

Acknowledgement

Project supported by the National Natural Science Foundation of China (Grant No. 52072132).

References

[1] Yu J, Loh X J, Luo Y, Ge S, Fan X and Ruan J 2020 *Biomater. Sci.* **8** 763
[2] Xie J, Gong L, Zhu S, Yong Y, Gu Z and Zhao Y 2019 *Adv. Mater.* **31** 1802244
[3] Yang Z, Kang S and Zhou R 2014 *Nanoscale* **6** 663
[4] Xu Y, Huang S W, Ding H M and Ma Y Q 2024 *Chin. Phys. B* **33** 028701
[5] Luo Y, Gu Z, Liao W, Huang Y and Luo Y 2024 *ACS Appl. Nano Mater.* **7** 3817
[6] Wu M, Ma H, Fang H, Yang L and Lei X 2023 *Chin. Phys. B* **32** 018701
[7] Ma H, Chen J, Fang H and Lei X 2021 *Chin. Phys. B* **30** 106806
[8] Zhang B Q and Shao Z G 2023 *Physica E* **146** 115547
[9] Calvaresi M and Zerbetto F 2013 *Acc. Chem. Res.* **46** 2454
[10] Zhang W, Huynh T, Xiu P, Zhou B, Ye C, Luan B and Zhou R 2015 *Carbon* **94** 895
[11] Gu Z, Song W, Chen S H, Li B, Li W and Zhou R 2019 *Nanoscale* **11** 19362
[12] Babadaei M M N, Moghaddam M F, Solhvand S, Alizadehmollayaghoob E, Attar F, Rajabbeigi E, Akhtari K, Sari S and Falahati M 2018 *Int. J. Nanomedicine* **13** 6871
[13] Bayda S, Amadio E, Cailotto S, Frión-Herrera Y, Perosa A and Rizzolio F 2021 *Nanoscale Adv.* **3** 5183
[14] Nel A, Xia T, Madler L and Li N 2006 *Science* **311** 622
[15] Carneiro P G, Pereira D G, da Silva B M O, Ribeiro H, Barbosa L A, Villar J A F P and Schnitzler M C 2023 *Surf. Interfaces* **41** 103211
[16] Albanese A, Tang P S and Chan W C 2012 *Annu. Rev. Biomed. Eng.* **14** 1
[17] An D Y, Su J G, Li C H and Li J Y 2015 *Chin. Phys. B* **24** 120504
[18] Wang J G, Shi X X, Liu Y R, Wang P Y, Chen H and Xie P 2022 *Chin. Phys. B* **31** 058702
[19] Tang Y, Yang Z, Yao Y, Zhou Y, Tan Y, Wang Z, Pan T, Xiong R, Sun J and Wei G 2024 *Chin. Phys. B* **33** 030701
[20] Jariwala D, Sangwan V K, Lauhon L J, Marks T J and Hersam M C 2013 *Chem. Soc. Rev.* **42** 2824
[21] Rao N, Singh R and Bashambu L 2021 *Mater. Today Proc.* **44** 608
[22] Hayashi T, Kim Y A, Natsuki T and Endo M 2007 *Chemphyschem* **8** 999
[23] Choi H and Yoon H 2015 *Nanomaterials* **5** 906
[24] Ispasoiu R G, Balogh L, Varnavski O P, Tomalia D A and Goodson 2000 *J. Am. Chem. Soc.* **122** 11005
[25] Wu J, Pan Z, Zhang Y, Wang B and Peng H 2018 *J. Mater. Chem. A* **6** 12932
[26] Qi X, Qin C, Zhong W, Au C, Ye X and Du Y 2010 *Materials* **3** 4142
[27] Lacerda L, Bianco A, Prato M and Kostarelos K 2006 *Adv. Drug. Deliv. Rev.* **58** 1460

[28] Chen X, Jiang X and Yang N 2022 *Small* **18** 2201135
[29] Niu X, Mao X, Yang D, Zhang Z, Si M and Xue D 2013 *Nanoscale Res. Lett.* **8** 1
[30] Bai H, Zhu Y, Qiao W and Huang Y 2011 *RSC Adv.* **1** 768
[31] Li G, Li Y, Liu H, Guo Y, Li Y and Zhu D 2010 *Chem. Commun.* **46** 3256
[32] He J, Li X, Lu T, Shen X, Wang N and Huang C 2019 *Dalton Trans.* **48** 14566
[33] Li Z Z 2015 *Carbon* **86** 301
[34] Wu Y, Chen X, Weng K, Arramel, Jiang J, Ong W J, Zhang P, Zhao X and Li N 2021 *Adv. Electron. Mater.* **7** 2001244
[35] Min H, Qi Y, Chen Y, Zhang Y, Han X, Xu Y, Liu Y, Hu J, Liu H, Li Y and Nie G 2019 *ACS Appl. Mater. Interfaces* **11** 32798
[36] Chen X and Zhang S 2018 *Acta Phys. Chim. Sin.* **34** 1061
[37] Liu J, Chen C and Zhao Y 2019 *Adv. Mater.* **31** 1804386
[38] Feng M, Bell D R, Luo J and Zhou R 2017 *Phys. Chem. Chem. Phys.* **19** 10187
[39] Gu Z, Yang Z, Luan B, Zhou X, Hong L, Zhou H, Luo J and Zhou R 2017 *J. Phys. Chem. C* **121** 2444
[40] Luan B, Huynh T and Zhou R 2016 *J. Phys. Chem. B* **120** 2124
[41] Zhu Z, Bai Q, Li S, Li S, Liu M, Du F, Sui N and Yu W W 2020 *Small* **16** 2001440
[42] Zuo G, Zhou X, Huang Q, Fang H and Zhou R 2011 *J. Phys. Chem. C* **115** 23323
[43] Li B, Li W, Perez-Aguilar J M and Zhou R 2017 *Small* **13** 1603685
[44] Luo Y, Gu Z, Perez-Aguilar J M, Liao W, Huang Y and Luo Y 2023 *Sci. Rep.* **13** 13783
[45] Gu Z, Perez-Aguilar J M, Meng L and Zhou R 2020 *J. Phys. Chem. B* **124** 7557
[46] Zhou M, Shen Q, Shen J W, Jin L, Zhang L, Sun Q, Hu Q and Liang L 2019 *Colloids Surf. B Biointerfaces* **174** 575
[47] Gu Z, Yang Z, Kang S, Yang J R, Luo J and Zhou R 2016 *Sci. Rep.* **6** 28252
[48] Zhang W, Gou Y, Cheng L, Dong K, Sheng Y, Ye C, Yang X and Mu Y 2023 *Phys. Chem. Chem. Phys.* **25** 3100
[49] Paul S and Biswas P 2023 *Phys. Chem. Chem. Phys.* **25** 26094
[50] Zhou M, Shen Q, Shen J W, Jin L, Zhang L, Sun Q, Hu Q and Liang L 2019 *Colloids Surf. B* **174** 575
[51] Jorgensen W L, Chandrasekhar J, Madura J D, Impey R W and Klein M L 1983 *J. Chem. Phys.* **79** 926
[52] Van Der Spoel D, Lindahl E, Hess B, Groenhof G, Mark A E and Berendsen H J 2005 *J. Comput. Chem.* **26** 1701
[53] Lindorff-Larsen K, Piana S, Palmo K, Maragakis P, Klepeis J L, Dror R O and Shaw D E 2010 *Proteins* **78** 1950
[54] Humphrey W, Dalke A and Schulten K 1996 *J. Mol. Graph.* **14** 33
[55] Essmann U, Perera L, Berkowitz M L, Darden T, Lee H and Pedersen L G 1995 *J. Chem. Phys.* **103** 8577
[56] Darden T, York D and Pedersen L 1993 *J. Chem. Phys.* **98** 10089
[57] Hess B, Bekker H, Berendsen H J and Fraaije J G 1997 *J. Comput. Chem.* **18** 1463
[58] Bussi G, Donadio D and Parrinello M 2007 *J. Chem. Phys.* **126** 014101
[59] Berendsen H J C, Postma J P M, van Gunsteren W F, DiNola A and Haak J R 1984 *J. Chem. Phys.* **81** 3684
[60] Kabsch W and Sander C 1983 *Biopolymers* **22** 2577
[61] Jha A K, Colubri A, Zaman M H, Koide S, Sosnick T R and Freed K F 2005 *Biochemistry* **44** 9691
[62] Laskowski R A, MacArthur M W, Moss D S and Thornton J M 1993 *J. Appl. Crystallogr.* **26** 283